https://doi.org/10.5194/egusphere-2024-2989
Preprint. Discussion started: 18 October 2024

Simple analytical–statistical models (ASMs) for mean annual permafrost table temperature and active-layer thickness estimates

Tomáš Uxa[1,2], Filip Hrbáček[2], and Michaela Kňažková[2]

[1]Institute of Geophysics, Czech Academy of Sciences, Prague, Czech Republic
[2]Polar-Geo-Lab, Department of Geography, Faculty of Science, Masaryk University, Brno, Czech Republic

Correspondence: Tomáš Uxa (uxa@ig.cas.cz)

Abstract. A variety of numerical, analytical and statistical models have been developed for estimating the mean annual permafrost table temperature (MAPT) and active-layer thickness (ALT). These tools typically require at least a few ground physical properties, such as thermal conductivity, heat capacity, water content or bulk density, as input parameters in addition to temperature variables, which are, however, unavailable or unrepresentative at most sites. Ground physical properties are therefore commonly estimated, which may yield model outputs of unknown validity. Hence, we devised two simple analytical–statistical models (ASMs) for estimating MAPT and ALT, which are driven solely by pairwise combinations of thawing and freezing indices in the active layer; no ground physical properties are required. ASMs reproduced MAPT and ALT well in most numerical validations, which corroborated their theoretical assumptions under idealized scenarios. Under field conditions of Antarctica and Alaska, the mean ASMs deviations in MAPT and ALT were less than 0.03 °C and 5 %, respectively, which is similar or better than other analytical or statistical models. This suggests that ASMs can be useful tools for estimating MAPT and ALT under a wide range of climates and ground physical conditions.

1 Introduction

Of ∼11 % of the Earth's exposed land surface underlain by permafrost (Obu, 2021), most seasonally thaws from the ground surface to a depth of up to several meters and then completely refreezes (active layer), which is mainly controlled by climate conditions and ground physical properties (Bonnaventure and Lamoureux, 2013). The active layer greatly influences the energy and mass transfer between the underlying permafrost, ground surface and the atmosphere, and is therefore critical for the dynamics of hydrologic, geomorphic, pedogenic, biologic and biogeochemic processes including greenhouse gas fluxes, as well as for human infrastructure in permafrost regions (e.g., Grosse et al., 2016; Walvoord and Kurylyk, 2016; Hjort et al., 2022). As climate is a first-order control on ground temperatures and thaw depth (Wang et al., 2019; Smith et al., 2022), the thermal state of permafrost and the thickness of the active layer have attracted a huge interest over recent decades because they are important measures of how the climate system is evolving (Li et al., 2022; Hrbáček et al., 2023b). Besides that, climate changes have provoked permafrost warming and active-layer thickening at a global scale (Biskaborn et al., 2019; Noetzli et al., 2024), which can have severe consequences on landscape and ecosystem stability as well as infrastructure integrity. Carbon release due to permafrost degradation is likely to trigger feedback mechanisms with impacts on the Earth's climate system

https://doi.org/10.5194/egusphere-2024-2989
Preprint. Discussion started: 18 October 2024

(Lawrence et al., 2015; Schuur et al., 2022). The permafrost and active-layer monitoring is therefore of utmost scientific and societal importance (Brown et al., 2000; Biskaborn et al., 2015).

The thermal state of permafrost and the thickness of the active layer have commonly been investigated by semi-continuous temperature measurements using data loggers with temperature sensors distributed in vertical arrays across the active layer and near-surface permafrost (e.g., Biskaborn et al., 2015; Noetzli et al., 2021), by periodic or semi-continuous geophysical measurements using electric, electromagnetic or seismic methods (e.g., Hauck, 2002; Farzamian et al., 2020), or by periodic thaw-depth measurements using physical probing with rigid rods or thaw-tube readings (e.g., Burn, 1998; Bonnaventure and Lamoureux, 2013). Of these methods, temperature measurements using data loggers are the most convenient in terms of accuracy, temporal resolution and/or logistics, which is well suitable for frequently remote and poorly accessible permafrost regions that have limited or no technical infrastructure (Brown et al., 2000; Biskaborn et al., 2015). At many places, however, temperatures are only measured in the active layer, and the permafrost temperatures and the active-layer thickness must therefore be estimated in these situations. This has been done using either statistical methods or numerical and analytical models of various complexity (e.g., Riseborough et al., 2008; Bonnaventure and Lamoureux, 2013; Aalto et al., 2018).

Of these solutions, analytical models in particular have become widely popular for estimating the mean annual temperature at the base of the active layer or the top of permafrost (hereafter referred to as the mean annual permafrost table temperature, MAPT) (Garagulya, 1990; Romanovsky and Osterkamp, 1995; Smith and Riseborough, 1996) and the active-layer thickness (ALT) (Neumann, c. 1860; Stefan, 1891; Kudryavtsev et al., 1977) because of their simplicity, small number of input parameters, computational efficiency and yet sufficient accuracy, which is highly advantageous for diverse permafrost regions and environmental settings (e.g., Anisimov et al., 1997; Nelson et al., 1997; Zhao et al., 2017; Obu et al., 2019, 2020). However, these tools require at least a few ground physical properties, such as thermal conductivity, heat capacity, water content or bulk density, as input parameters in addition to temperature variables, which are seldom available at most sites. Ground physical properties are therefore commonly estimated, which may yield model outputs of unknown validity. But even in-situ measurements of ground physical properties may not guarantee accurate model outputs either, as they are usually taken annually or less frequently and are then typically treated as constants in models, regardless of their temporal variability (e.g., Gao et al., 2020; Hrbáček et al., 2023a; Li et al., 2023; Kňažková and Hrbáček, 2024; Wenhao et al., 2024).

Here, we devise two novel analytical–statistical models (ASMs) for MAPT and ALT, which are driven solely by thawing and freezing indices at two distinct depths in the active layer to address the general lack and/or non-representativeness of ground physical data for permafrost models. We test these solutions against numerical model simulations for idealized scenarios as well as against field observations from distinct permafrost environments of Antarctica and Alaska, and we discuss their performance, advantages and limitations.

https://doi.org/10.5194/egusphere-2024-2989
Preprint. Discussion started: 18 October 2024

2 Model derivations

2.1 Mean annual permafrost table temperature

Besides other solution (Garagulya, 1990), MAPT [°C] can be calculated by the TTOP model (Romanovsky and Osterkamp, 1995; Smith and Riseborough, 1996), which assumes that the ratio of thawed and frozen thermal conductivity and the effects of latent heat produce the difference between MAPT and the mean annual ground surface temperature (thermal offset). The TTOP formula for permafrost conditions (MAPT ≤ 0 °C) is as follows (Romanovsky and Osterkamp, 1995; Smith and Riseborough, 1996)

$$\mathrm{MAPT} = \frac{\frac{k_t}{k_f} I_{ts} - I_{fs}}{P}, \tag{1}$$

where k_t [W m^{-1} K^{-1}] and k_f [W m^{-1} K^{-1}] is the thawed and frozen thermal conductivity, respectively, I_{ts} [°C d] and I_{fs} [°C d] is the ground surface thawing and freezing index, respectively (both expressed degree-days and in absolute values), and P [365 d] is the length of one year.

Besides surface temperatures, Eq. (1) is valid for temperatures measured at any depth in the active layer, which is highly convenient because ground surface temperature is difficult to measure due to surface radiative and convective energy fluxes and due to problematic fixing of temperature sensors exactly at the ground surface level (Riseborough, 2003). Hence, MAPT based on temperatures measured at two distinct depths in the active layer z_1 and z_2 ($z_1 < z_2 <$ ALT) can be expressed as follows

$$\mathrm{MAPT} = \frac{\frac{k_t}{k_f} I_{tz_1} - I_{fz_1}}{P}, \tag{2}$$

$$\mathrm{MAPT} = \frac{\frac{k_t}{k_f} I_{tz_2} - I_{fz_2}}{P}, \tag{3}$$

where I_{tz_1} [°C d] and I_{fz_1} [°C d] is the thawing and freezing index, respectively, at the depth z_1, and I_{tz_2} [°C d] and I_{fz_2} [°C d] is the thawing and freezing index, respectively, at the depth z_2. This implies that Eq. (2) and (3) are equivalent:

$$\frac{\frac{k_t}{k_f} I_{tz_1} - I_{fz_1}}{P} = \frac{\frac{k_t}{k_f} I_{tz_2} - I_{fz_2}}{P}. \tag{4}$$

Solving Eq. (4) for the thermal conductivity ratio yields

$$\frac{k_t}{k_f} = \frac{I_{fz_1} - I_{fz_2}}{I_{tz_1} - I_{tz_2}}. \tag{5}$$

Equation (5) can be then substituted for the thermal conductivity ratio in Eq. (2) and (3) as follows

$$\mathrm{MAPT} = \frac{\frac{I_{fz_1} - I_{fz_2}}{I_{tz_1} - I_{tz_2}} I_{tz_1} - I_{fz_1}}{P}, \tag{6}$$

$$\mathrm{MAPT} = \frac{\frac{I_{fz_1} - I_{fz_2}}{I_{tz_1} - I_{tz_2}} I_{tz_2} - I_{fz_2}}{P}. \tag{7}$$

https://doi.org/10.5194/egusphere-2024-2989
Preprint. Discussion started: 18 October 2024

Subsequently, Eq. (6) and (7) both simplify to the same formula for MAPT:

$$\mathrm{MAPT} = \frac{\frac{I_{fz_1} I_{tz_2} - I_{fz_2} I_{tz_1}}{I_{tz_1} - I_{tz_2}}}{P}. \tag{8}$$

Substantially, Eq. (8) implies that MAPT can be simply estimated using thawing and freezing indices at two distinct depths in the active layer alone, that is, without the knowledge of the thermal conductivity ratio.

While Eq. (8) has a physical basis, it can be shown that it is in principle a linear extrapolation of the freezing index to the depth where the thawing index becomes zero, with the slope defined by the thermal conductivity ratio, and its division by the length of one year. Using the same notation as before, this can be expressed as follows

$$\frac{I_{fz_1} - I_{f_{\mathrm{ALT}}}}{I_{tz_1} - I_{t_{\mathrm{ALT}}}} = \frac{I_{fz_1} - I_{fz_2}}{I_{tz_1} - I_{tz_2}}, \tag{9}$$

$$\frac{I_{fz_2} - I_{f_{\mathrm{ALT}}}}{I_{tz_2} - I_{t_{\mathrm{ALT}}}} = \frac{I_{fz_1} - I_{fz_2}}{I_{tz_1} - I_{tz_2}}, \tag{10}$$

where $I_{t_{\mathrm{ALT}}}$ [°C d] and $I_{f_{\mathrm{ALT}}}$ [°C d] represents the thawing and freezing index at the base of the active layer. Solving Eq. (9) and (10) for $I_{f_{\mathrm{ALT}}}$ gives

$$-I_{f_{\mathrm{ALT}}} = \frac{I_{fz_1} - I_{fz_2}}{I_{tz_1} - I_{tz_2}} (I_{tz_1} - I_{t_{\mathrm{ALT}}}) - I_{fz_1}, \tag{11}$$

$$-I_{f_{\mathrm{ALT}}} = \frac{I_{fz_1} - I_{fz_2}}{I_{tz_1} - I_{tz_2}} (I_{tz_2} - I_{t_{\mathrm{ALT}}}) - I_{fz_2}. \tag{12}$$

Since the thawing index at the base of the active layer is zero, Eq. (11) and (12) become equivalent to Eq. (6) and (7), respectively, when divided by the length of one year, and both simplify to Eq. (8). This documents that Eq. (8) for MAPT is analytical and statistical at the same time because it integrates both approaches.

2.2 Active-layer thickness

Besides other solutions (Neumann, c. 1860; Kudryavtsev et al., 1977), ALT [m] can be calculated by the Stefan (1891) model, which builds on the premise that the conductive heat flux above the thaw front equals to the rate at which latent heat is absorbed as the thaw front propagates downwards. Its simplest is as follows (Lunardini, 1981)

$$\mathrm{ALT} = \sqrt{\frac{2 k_t I_{ts}}{L \phi}}, \tag{13}$$

where L [3.34×10^8 J m^{-3}] is the volumetric latent heat of fusion of water and ϕ [–] is the volumetric water content. Note that the thawing index must be multiplied by the scaling factor of 86 400 s d^{-1} in the Stefan model to yield correct outputs. As stated previously (Sect. 2.1), the ground surface temperature is difficult to measure (Riseborough, 2003), and therefore the Stefan model has commonly been forced by temperatures recorded at some depth in the active layer. However, this has rarely been accounted for, although it has been shown to substantially affect the model outputs (Hrbáček and Uxa, 2020; Kaplan Pastíriková et al., 2023), and can be easily implemented as follows (Riseborough, 2003; Hayashi et al., 2007)

$$\mathrm{ALT} = z + \sqrt{\frac{2 k_t I_{tz}}{L \phi}}, \tag{14}$$

https://doi.org/10.5194/egusphere-2024-2989
Preprint. Discussion started: 18 October 2024

where z [m] represents the depth where the forcing temperature was measured and I_{tz} [°C d] is the thawing index at the depth z. ALT estimated using thawing indices measured at two distinct depths in the active layer z_1 and z_2 ($z_1 < z_2 <$ ALT) can be expressed as follows

$$\mathrm{ALT} = z_1 + \sqrt{\frac{2k_t I_{tz_1}}{L\phi}}, \tag{15}$$

$$\mathrm{ALT} = z_2 + \sqrt{\frac{2k_t I_{tz_2}}{L\phi}}. \tag{16}$$

This implies that Eq. (15) and (16) are equivalent:

$$z_1 + \sqrt{\frac{2k_t I_{tz_1}}{L\phi}} = z_2 + \sqrt{\frac{2k_t I_{tz_2}}{L\phi}}. \tag{17}$$

The vertical distance between z_2 and z_1 can be expressed as

$$z_2 - z_1 = \sqrt{\frac{2k_t I_{tz_1}}{L\phi}} - \sqrt{\frac{2k_t I_{tz_2}}{L\phi}}, \tag{18}$$

which simplifies to

$$z_2 - z_1 = \sqrt{\frac{2k_t}{L\phi}}\left(\sqrt{I_{tz_1}} - \sqrt{I_{tz_2}}\right). \tag{19}$$

Subsequently rearranging Eq. (19) gives

$$\frac{z_2 - z_1}{\sqrt{I_{tz_1}} - \sqrt{I_{tz_2}}} = \sqrt{\frac{2k_t}{L\phi}}, \tag{20}$$

where the right-hand side corresponds to the so-called edaphic term, which has previously been used in numerous studies (Nelson and Outcalt, 1987; Hinkel and Nicholas, 1995; Nelson et al., 1997; Anisimov et al., 2002; Shiklomanov and Nelson, 2002; Shiklomanov et al., 2010; de Pablo et al., 2018; Peng et al., 2023) to combine the ground physical properties in the Stefan model into a single variable as follows

$$\mathrm{ALT} = E\sqrt{I_{tz}}, \tag{21}$$

where E [m s$^{-0.5}$ K$^{-0.5}$] denotes the edaphic term given by

$$E = \sqrt{\frac{2k_t}{L\phi}}. \tag{22}$$

Usually, Eq. (21) has been referred to as the modified Stefan model and proved to be useful in situations where the ground physical properties were unavailable and/or for spatial modelling of ALT (Nelson and Outcalt, 1987; Hinkel and Nicholas, 1995; Nelson et al., 1997; Anisimov et al., 2002; Shiklomanov and Nelson, 2002; Shiklomanov et al., 2010; Peng et al., 2023).

https://doi.org/10.5194/egusphere-2024-2989
Preprint. Discussion started: 18 October 2024

Its major advantage is that it can largely overcome many of the shortcomings of the simplistic Stefan model (Eq. 13), which assumes that the ground physical properties throughout the active layer are constant, the active-layer temperature decreases linearly from the surface to the bottom frozen layer that is at 0 °C, and the conductive heat flux is fully consumed by latent heat to thaw the active layer (Kurylyk, 2015). However, the value of the edaphic term has only been derived based on empirical relationships between ALT and thawing index in several thawing seasons and/or at multiple locations (Nelson et al., 1997; Anisimov et al., 2002; Shiklomanov and Nelson, 2002; Peng et al., 2023). This led on the one hand to its high accuracy for the calibration conditions, but on the other hand had limitations in terms of its transferability to other thawing seasons and/or locations. Notwithstanding that, the edaphic term can be implemented in Eq. (15) and (16) as follows

$$\mathrm{ALT} = z_1 + E\sqrt{I_{tz_1}}, \tag{23}$$

$$\mathrm{ALT} = z_2 + E\sqrt{I_{tz_2}}. \tag{24}$$

Substituting the left-hand side of Eq. (20) for the edaphic term in Eq. (23) and (24) yields

$$\mathrm{ALT} = z_1 + \frac{z_2 - z_1}{\sqrt{I_{tz_1}} - \sqrt{I_{tz_2}}}\sqrt{I_{tz_1}}, \tag{25}$$

$$\mathrm{ALT} = z_2 + \frac{z_2 - z_1}{\sqrt{I_{tz_1}} - \sqrt{I_{tz_2}}}\sqrt{I_{tz_2}}. \tag{26}$$

Simplifying Eq. (25) and (26) then produces the same formula for ALT:

$$\mathrm{ALT} = \frac{z_2\sqrt{I_{tz_1}} - z_1\sqrt{I_{tz_2}}}{\sqrt{I_{tz_1}} - \sqrt{I_{tz_2}}}. \tag{27}$$

Substantially, Eq. (27) implies that ALT can be simply estimated using thawing indices at two distinct depths in the active layer alone, that is, without the knowledge of the ground physical properties or the edaphic term.

While Eq. (27) has a physical basis, it can also be shown that it is in principle a linear extrapolation of the depth at which the square root of the thawing indices becomes zero (cf. Riseborough, 2003), with the slope defined by the edaphic term. Using the same notation as before, this can be expressed as follows

$$\frac{\mathrm{ALT} - z_1}{\sqrt{I_{tz_1}} - \sqrt{I_{t_{\mathrm{ALT}}}}} = \frac{z_2 - z_1}{\sqrt{I_{tz_1}} - \sqrt{I_{tz_2}}}, \tag{28}$$

$$\frac{\mathrm{ALT} - z_2}{\sqrt{I_{tz_2}} - \sqrt{I_{t_{\mathrm{ALT}}}}} = \frac{z_2 - z_1}{\sqrt{I_{tz_1}} - \sqrt{I_{tz_2}}}. \tag{29}$$

Solving Eq. (28) and (29) for ALT gives

$$\mathrm{ALT} = z_1 + \frac{z_2 - z_1}{\sqrt{I_{tz_1}} - \sqrt{I_{tz_2}}}\left(\sqrt{I_{tz_1}} - \sqrt{I_{t_{\mathrm{ALT}}}}\right), \tag{30}$$

$$\mathrm{ALT} = z_2 + \frac{z_2 - z_1}{\sqrt{I_{tz_1}} - \sqrt{I_{tz_2}}}\left(\sqrt{I_{tz_2}} - \sqrt{I_{t_{\mathrm{ALT}}}}\right). \tag{31}$$

Since the thawing index at the base of the active layer is zero, Eq. (30) and (31) are equivalent to Eq. (25) and (26), respectively, and both simplify to Eq. (27). As with Eq. (8), this documents that Eq. (27) for ALT is analytical and statistical at the same time because it integrates both approaches.

https://doi.org/10.5194/egusphere-2024-2989
Preprint. Discussion started: 18 October 2024

3 Model validations

The validity of ASMs for estimating MAPT and ALT given by Eq. (8) and (27), respectively, was tested in a twofold manner, with ground temperatures simulated by a simple one-dimensional numerical model for idealized scenarios and those from field observations.

3.1 Idealized scenarios

We considered five scenarios with a mean annual air temperature (MAAT) of −12 °C, −10 °C, −8 °C, −6 °C and −4 °C that varied sinusoidally over a year within a range of 40 °C. The air temperatures were converted to ground surface temperature series using linear scaling with so-called thawing and freezing *n*-factors of 1 and 0.5, respectively (Lunardini, 1978). Ground temperatures were then simulated using a one-dimensional numerical model by solving the transient heat conduction equation with phase changes (Carslaw and Jaeger, 1959):

$$C_{\text{eff}} \frac{\partial T}{\partial t} = \frac{\partial}{\partial z}\left(k \frac{\partial T}{\partial z}\right), \tag{32}$$

where C_{eff} [J m^{-3} K^{-1}] is the apparent volumetric heat capacity, T [°C] is the temperature, t [s] is the time, and k [W m^{-1} K^{-1}] is the thermal conductivity. Ground was set to be fully frozen and thawed at T_f [−0.05 °C] and T_t [0.05 °C], respectively, and linear intermediate in between. Although simplistic, this was chosen to be as close as possible to ASMs, which assume a water—ice transition at 0 °C, while ensuring numerical stability. Similar to Sun et al. (2020), the apparent volumetric heat capacity and thermal conductivity accounted for phase changes with latent heat effects as follows

$$C_{\text{eff}} = \begin{cases} C_f & \text{for } T \le T_f \\ C_f + (C_t - C_f)\,\frac{T - T_f}{T_t - T_f} + \frac{L\phi}{T_t - T_f} & \text{for } T_f < T \le T_t \\ C_t & \text{for } T > T_t \end{cases}, \tag{33}$$

$$k = \begin{cases} k_f & \text{for } T \le T_f \\ k_f + (k_t - k_f)\,\frac{T - T_f}{T_t - T_f} & \text{for } T_f < T \le T_t \\ k_t & \text{for } T > T_t \end{cases}, \tag{34}$$

where C_f [J m^{-3} K^{-1}] and C_t [J m^{-3} K^{-1}] is the frozen and thawed volumetric heat capacity, respectively. The values of the frozen thermal conductivity and the frozen volumetric heat capacity were estimated from the thawed ones based on the volumetric water content as follows (Nicolsky et al., 2009)

$$k_f = k_t \left(\frac{k_i}{k_w}\right)^{\phi}, \tag{35}$$

$$C_f = C_t - \phi\,(C_w - C_i), \tag{36}$$

where k_i [2.22 W m^{-1} K^{-1}] is the thermal conductivity of ice, k_w [0.57 W m^{-1} K^{-1}] is the thermal conductivity of water, C_w [4.21×10^6 J m^{-3} is the volumetric heat capacity of water, and C_i [2.05×10^6 J m^{-3} K^{-1}] is the volumetric heat capacity of ice.

https://doi.org/10.5194/egusphere-2024-2989
Preprint. Discussion started: 18 October 2024

Table 1. Values of ground physical properties used in the numerical model simulations for idealized scenarios.

Variable	Value	Unit
Peat		
Depth	0–0.2	m
Thawed thermal conductivity	0.50	$W\,m^{-1}\,K^{-1}$
Frozen thermal conductivity	0.92	$W\,m^{-1}\,K^{-1}$
Thawed volumetric heat capacity	2.300×10^{6}	$J\,m^{-3}\,K^{-1}$
Frozen volumetric heat capacity	1.328×10^{6}	$J\,m^{-3}\,K^{-1}$
Volumetric water content	45	%
Mineral soil		
Depth	>0.2	m
Thawed thermal conductivity	1.50	$W\,m^{-1}\,K^{-1}$
Frozen thermal conductivity	2.26	$W\,m^{-1}\,K^{-1}$
Thawed volumetric heat capacity	2.500×10^{6}	$J\,m^{-3}\,K^{-1}$
Frozen volumetric heat capacity	1.852×10^{6}	$J\,m^{-3}\,K^{-1}$
Volumetric water content	30	%

One- and two-layer profiles representing mineral soil alone and 20 cm of peat over mineral soil, respectively, that had constant physical properties except for phase changes were considered in these numerical tests (Table 1), as they aimed to demonstrate the viability of ASMs under idealized conditions. Since ASMs assume a homogeneous profile, the two-layer profile was to examine their behaviour when this condition is not met.

The numerical model was solved using an implicit finite-difference scheme for a 100 m deep domain, which was discretized so that the computation nodes were closely spaced in the active layer and shallow permafrost for the most accurate outputs there, while their density decreased towards the deepest node where the temperature remained stable. Specifically, the node spacing was 0.01 m, 0.1 m, 0.5 m, 1 m, 5 m and 10 m in the depth intervals of 0–2 m, 2–5 m, 5–10 m, 10–20 m, 20–50 m and 50–100 m, respectively. At the upper boundary, the model was forced by the ground surface temperatures. A zero heat flux was set at the lower boundary. The initial temperature was established by Eq. (1) using thawing and freezing indices at the ground surface and at the bottom of the top peat layer for the one- and two-layer profiles, respectively, in order to speed up the time to reach the steady-state conditions throughout the model domain. The model was run for 50 years with a time step of 1 hour to ensure that the simulated temperatures are not affected by the initial conditions. Steady-state MAPT, ALT, and thawing and freezing indices simulated for the last year were then used for numerical validations of ASMs given by Eq. (8) and (27).

https://doi.org/10.5194/egusphere-2024-2989
Preprint. Discussion started: 18 October 2024

Table 2. List of the Antarctic and Alaskan sites and the number of years/seasons used for the model validations.

Site	Latitude [°]	Longitude [°]	Altitude [m asl]	Validation period	Years for MAPT	Seasons for ALT
James Ross Island						
Abernethy Flats	−63.88138	−57.94832	41	2013–2020	6–6	7–7
Berry Hill slopes	−63.80267	−57.83863	56	2017–2020	3–3	3–3
CALM	−63.80190	−57.88460	10	2014–2023	7–7	8–8
Johann Gregor Mendel	−63.80152	−57.88330	10	2011–2023	10–12	11–12
Johnson Mesa	−63.82250	−57.93280	340	2012–2023	8–11	9–11
McMurdo Sound						
Bull Pass	−77.51847	161.86269	141	1999–2022	15–22	14–22
Granite Harbour	−77.00655	162.52561	6	2007–2017	4–4	5–5
Marble Point	−77.41955	163.68247	47	1999–2022	18–22	17–21
North Slope of Alaska						
Atqasuk	70.45242	−157.41178	22	1998–2010	6–9	8–12
Barrow (site 1)	71.32242	−156.61089	9	1997–2017	15–16	15–17
Betty Pingo: polygon center	70.28258	−148.89347	12	2006–2022	0–9	0–9
Betty Pingo: polygon rim	70.28258	−148.89347	12	2006–2012	4–7	4–7
Westdock (high): polygon center	70.37039	−148.56867	3	2002–2020	16–17	18–19
Westdock (high): polygon rim	70.37039	−148.56867	3	2003–2020	16–17	18–18
Westdock (high): polygon trough	70.37039	−148.56867	3	2003–2020	9–17	11–18
Westdock (low): polygon center	70.37047	−148.56561	2	2004–2011	4–4	8–8
Westdock (low): polygon trough	70.37047	−148.56561	2	2004–2022	1–9	6–13

3.2 Field observations

Ground temperatures were collected for 17 sites situated in permafrost environments on James Ross Island and McMurdo Sound in Antarctica and on the North Slope of Alaska in the Arctic (Table 2) in order to test ASMs under diverse climates and ground physical conditions. A total of 142–192 and 162–210 years/seasons (Table 2) with quality-checked observations of MAPT, ALT, and thawing and freezing indices were available for individual validation scenarios of ASMs given Eq. (8) and (27), respectively, (see Sect. 3.3). The variability in the number of available years/seasons for the validations (Table 2) was because in some years/seasons the active layer was thinner than the deepest sensors used in Eq. (8) and (27) and/or due to data gaps.

https://doi.org/10.5194/egusphere-2024-2989
Preprint. Discussion started: 18 October 2024

3.3 Model evaluation

For both numerical and field validations of ASMs, the thawing and freezing indices were calculated as annual sums of positive and negative mean daily ground temperatures, respectively, and for convenience expressed in degree-days and in absolute values. textrmALT was derived as the maximum seasonal depth of the 0 °C isotherm by a linear interpolation of the depths where the mean daily ground temperatures were just above and below 0 °C. Subsequently, the mean annual temperatures at the same depths were used to interpolate MAPT. We used three pairwise combinations of thawing and freezing indices at the depth of 5 cm, 30 cm and 50 cm as inputs of Eq. (8) and (27) for numerical validations, while thawing and freezing indices from the depth intervals of 0–10 cm, 25–35 cm and 45–55 cm (for convenience hereafter also referred to as 5 cm, 30 cm and 50 cm) were considered for field validations because the sensor depths differ at individual sites. However, this did not compromise the consistency of field validations and allowed us to reveal which depth combinations and in which portion of the active layer worked best. The ASMs outputs were compared with MAPT and ALT from the numerical model simulations and field observations and evaluated using common error metrics, such as the mean error (ME), the mean percentage error (MPE), the mean absolute error (MAE), the mean absolute percentage error (MAPE), and the root-mean-square error (RMSE).

4 Results

4.1 Mean annual permafrost table temperature

4.1.1 Numerical validation

The numerical model simulations for the five MAAT scenarios showed that the thawing and freezing indices tend to decrease exponentially from the ground surface towards the base of the active layer where the thawing indices are zero (Fig. 1). However, the relationships between the thawing and freezing indices themselves are linear within each subsurface layer (both peat and mineral soil), and their slopes are governed by the thermal conductivity ratios in the individual layers (Fig. 2).

MAPT estimated by Eq. (8) based on the numerically modelled thawing and freezing indices at the depth pairs of 5/30 cm, 5/50 cm and 30/50 cm for the five MAAT scenarios showed almost perfect agreement with MAPT simulated by the numerical model in the one-layer profiles (Table 3), as ME was −0.003 °C to −0.002 °C, MAE was 0.002 °C to 0.003 °C, and RMSE was 0.002 °C to 0.003 °C. The accuracy of Eq. (8) was slightly lower in the two-layer profiles (Table 3), as ME was −0.105 °C to −0.003 °C, MAE was 0.003 °C to 0.105 °C, and RMSE was 0.004 °C to 0.124 °C.

Overall, however, these findings corroborate the theoretical assumptions outlined in Sect. 2.1 and justify ASM given by Eq. (8) for estimating MAPT under the idealized scenarios.

4.1.2 Field validation

MAPT estimated by Eq. (8) based on the thawing and freezing indices at the depth pairs 5/30 cm, 5/50 cm and 30/50 cm at the Antarctic and Alaskan sites yielded the site-weighted ME of 0.02 °C to 0.03 °C compared to the observed MAPT (Fig. 3).

https://doi.org/10.5194/egusphere-2024-2989
Preprint. Discussion started: 18 October 2024

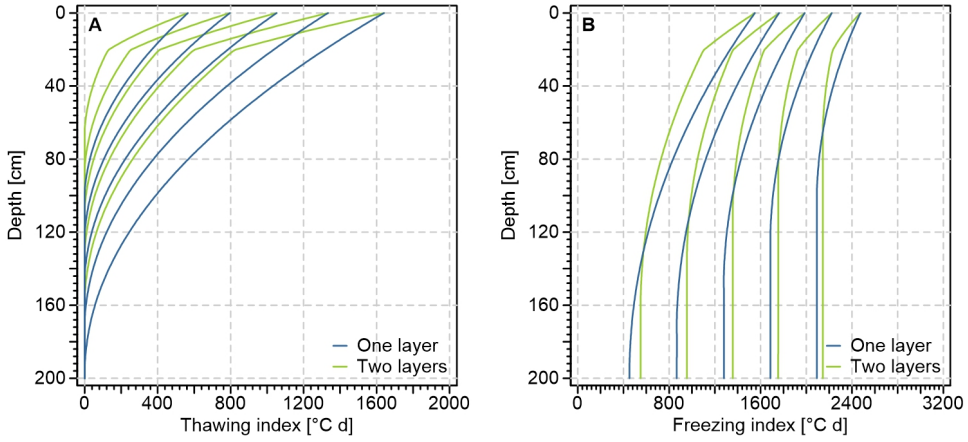

Figure 1. Depth profiles of (A) the thawing indices and (B) the freezing indices in the active layer and near-surface permafrost simulated by the numerical model for MAAT of −12 °C, −10 °C, −8 °C, −6 °C and −4 °C that varied sinusoidally over a year within a range of 40 °C. Note the bent shapes of the thawing and freezing indices in the active layer, which only change abruptly at the interface of peat and mineral soil in the two-layer profiles due to distinct physical properties of these materials (see Table 1).

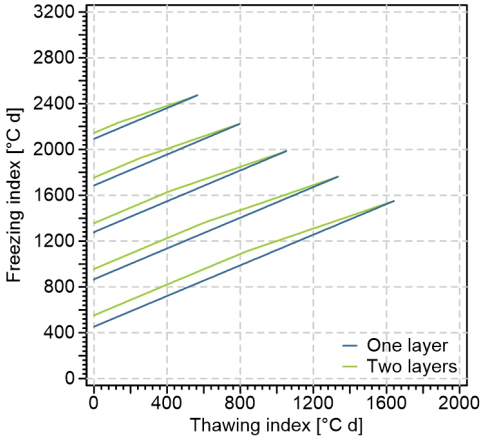

Figure 2. Relationships between the thawing and freezing indices in the active layer simulated by the numerical model for MAAT of −12 °C, −10 °C, −8 °C, −6 °C and −4 °C that varied sinusoidally over a year within a range of 40 °C. Note that the relationships are linear, but their slopes change abruptly at the interface of peat and mineral soil in the two-layer profiles due to distinct physical properties of these materials (see Table 1).

Since the errors were scattered around zero (Fig. 3), the site-weighted MAE was somewhat larger of 0.08 °C to 0.14 °C and the site-weighted RMSE was 0.10 °C to 0.17 °C (Fig. 3). The majority of the errors was within ±0.2 °C (Fig. 3).

The accuracy of the ASM estimates was slightly lower in Antarctica (Fig. 3) where the site-weighted ME was −0.04 °C to 0.04 °C, the site-weighted MAE was 0.10 °C to 0.15 °C, and the site-weighted RMSE was 0.13 °C to 0.18 °C. In Alaska, the

https://doi.org/10.5194/egusphere-2024-2989
Preprint. Discussion started: 18 October 2024

Table 3. Comparison of MAPT simulated by the numerical model for MAAT of −12 °C, −10 °C, −8 °C, −6 °C and −4 °C that varied sinusoidally over a year within a range of 40 °C and MAPT estimated with ASM given by Eq. (8) based on the numerically modelled thawing and freezing indices at the depth pairs of 5/30 cm, 5/50 cm and 30/50 cm.

Scenario	MAAT [°C]	$MAPT_{num}$ [°C]	$MAPT_{5/30}$ [°C]	$MAPT_{5/50}$ [°C]	$MAPT_{30/50}$ [°C]
One layer	−4	−1.24	−1.25	−1.25	−1.25
	−6	−2.38	−2.38	−2.38	−2.38
	−8	−3.50	−3.51	−3.51	−3.51
	−10	−4.62	−4.62	−4.62	−4.62
	−12	−5.73	−5.73	−5.73	−5.73
	Mean	−3.49	−3.50	−3.50	−3.50
Two layers	−4	−1.51	−1.72	−1.63	−1.52
	−6	−2.62	−2.77	−2.70	−2.62
	−8	−3.72	−3.81	−3.76	−3.72
	−10	−4.81	−4.86	−4.83	−4.81
	−12	−5.88	−5.90	−5.88	−5.88
	Mean	−3.71	−3.81	−3.76	−3.71

site-weighted ME was −0.01 °C to 0.09 °C, the site-weighted MAE was 0.07 °C to 0.13 °C, and the site-weighted RMSE was 0.08 °C to 0.15 °C. However, the ASM deviations exhibited very similar distributions in both regions (Fig. 1).

4.2 Active-layer thickness

4.2.1 Numerical validation

As stated in Sect. 4.1.1, the numerical model simulations for the five MAAT scenarios showed that the thawing indices tend to decrease exponentially from the ground surface towards the base of the active layer where they are zero (Fig. 1A). If square rooted, however, the bent-shaped depth profiles of the thawing indices become linear within each subsurface layer (both peat and mineral soil), except for subtle deviations near the base of the active layer, and their slopes are governed by the edaphic terms in the individual layers (Fig. 4).

ALT estimated by Eq. (27) based on the numerically modelled thawing indices at the depth pairs of 5/30 cm, 5/50 cm and 30/50 cm for the five MAAT scenarios was well consistent with ALT simulated by the numerical model in the one-layer profiles (Table 4), as ME was 0.8 cm (0.9 %) to 1.8 cm (1.5 %), MAE was 1.6 cm (1.3 %) to 1.8 cm (1.5 %), and RMSE was 1.6 cm to 1.9 cm. On the other hand, the accuracy of Eq. (27) was much worse in the two-layer profiles when the thawing indices from the top peat layer were used for the calculations (Table 4), as ME was −41.0 cm (−35.4 %) to 2.4 cm (2.7 %), MAE was 2.4 cm (2.7 %) to 41.0 cm (35.4 %), and RMSE was 3.4 cm to 35.9 cm. The deviations tended to decrease as the active layer thickened in the one-layer profiles, while they tended to increase as the active-layer thickened in the two-layer profiles (Table 4).

https://doi.org/10.5194/egusphere-2024-2989
Preprint. Discussion started: 18 October 2024

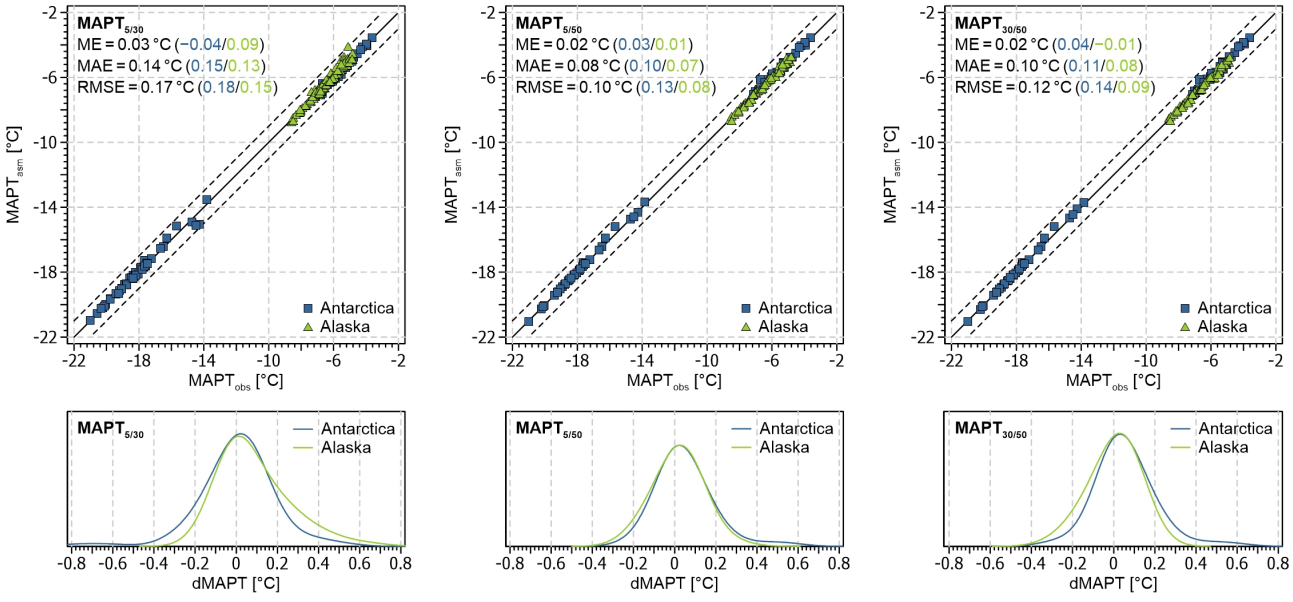

Figure 3. (Upper row) Comparison of MAPT observed at the Antarctic and Alaskan sites and MAPT estimated with ASM given by Eq. (8) based on the observed thawing and freezing indices at the depth pairs of 5/30 cm, 5/50 cm and 30/50 cm. The blue and green numbers in parentheses indicate the mean errors for the Antarctic and Alaskan sites, respectively. The black solid and dashed lines represent the line of identity and the deviation of ±1 °C, respectively. (Lower row) Probability distribution of the errors in MAPT estimated with ASM for the depth pairs of 5/30 cm, 5/50 cm and 30/50 cm.

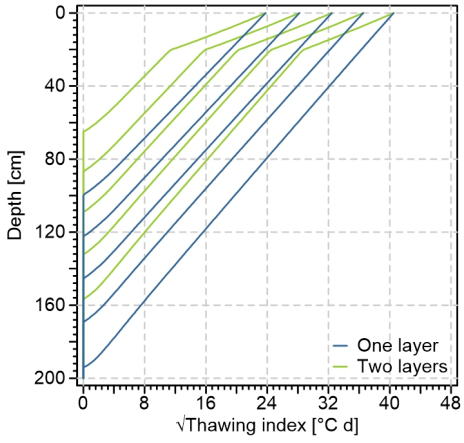

Figure 4. Depth profiles of the square-rooted thawing indices in the active layer and near-surface permafrost simulated by the numerical model for MAAT of −12 °C, −10 °C, −8 °C, −6 °C and −4 °C that varied sinusoidally over a year within a range of 40 °C. Note that the bent shapes of the thawing indices (Fig. 1A) become linear when square-rooted, but their slopes change abruptly at the interface of peat and mineral soil in the two-layer profiles due to distinct physical properties of these materials (see Table 1).

https://doi.org/10.5194/egusphere-2024-2989
Preprint. Discussion started: 18 October 2024

Table 4. Comparison of ALT simulated by the numerical model for MAAT of −12 °C, −10 °C, −8 °C, −6 °C and −4 °C that varied sinusoidally over a year within a range of 40 °C and ALT estimated with ASM given by Eq. (27) based on the numerically modelled thawing and freezing indices at the depth pairs of 5/30 cm, 5/50 cm and 30/50 cm.

Scenario	MAAT [°C]	ALT_{num} [cm]	$ALT_{5/30}$ [cm]	$ALT_{5/50}$ [cm]	$ALT_{30/50}$ [cm]
One layer	−4	195	193	194	195
	−6	170	170	170	171
	−8	146	147	148	148
	−10	123	125	126	126
	−12	100	103	103	103
	Mean	146.8	147.6	148.2	148.6
Two layers	−4	157	90	116	158
	−6	133	79	102	134
	−8	109	69	88	112
	−10	87	59	75	90
	−12	65	49	62	69
	Mean	110.2	69.2	88.6	112.6

Overall, however, these findings corroborate the theoretical assumptions outlined in Sect. 2.2 and justify ASM given by Eq. (27) for estimating ALT under idealized scenarios in one-layer profiles.

4.2.2 Field validation

ALT estimated by Eq. (27) based on the thawing indices at the depth pairs of 5/30 cm, 5/50 cm and 30/50 cm at the Antarctic and Alaskan sites showed the site-weighted ME of −2.6 cm (−4.4 %) to −1.4 cm (−2.4 %) compared to the observed ALT (Fig. 5). The site-weighted MAE was somewhat larger, as it attained 4.8 cm (6.9 %) to 8.8 cm (13.5 %), while the site-weighted RMSE was 5.3 cm to 9.8 cm (Fig. 5).

ALT estimates by Eq. (27) were more accurate in Antarctica where the site-weighted ME was 0.9 cm (0.8 %) to 5.4 cm (7.2 %), the site-weighted MAE was 3.5 cm (4.6 %) to 8.4 cm (11.9 %), and the site-weighted RMSE was 4.0 cm to 9.7 cm. By contrast, in Alaska the site-weighted ME was −8.6 cm (−13.9 %) to −3.6 cm (−5.6 %), the site-weighted MAE was 5.2 cm (8.2 %) to 9.1 cm (14.9 %), and the site-weighted RMSE was 5.8 cm to 10.0 cm. The ASM deviations were roughly scattered around zero in Antarctica, while they tended to be negative in Alaska where the deviations also exhibited a bimodal distribution for the depth pair of 5/30 cm (Fig. 5).

https://doi.org/10.5194/egusphere-2024-2989
Preprint. Discussion started: 18 October 2024

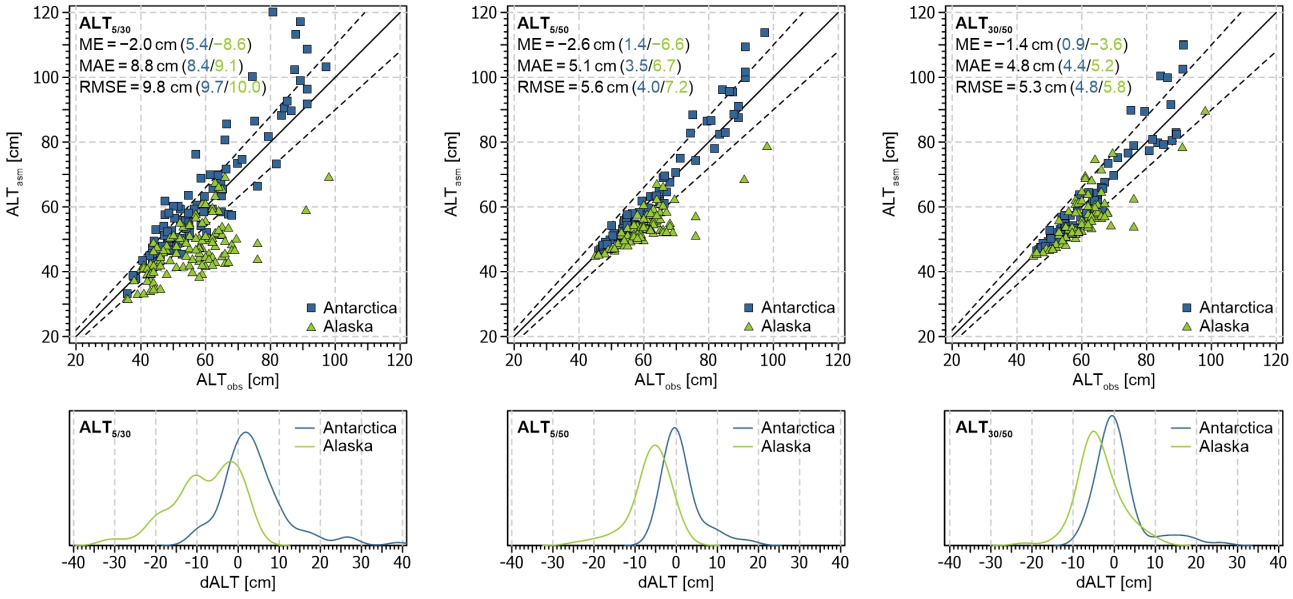

Figure 5. (Upper row) Comparison of ALT observed at the Antarctic and Alaskan sites and ALT estimated with ASM given by Eq. (27) based on the observed thawing indices at the depth pairs of 5/30 cm, 5/50 cm and 30/50 cm. The blue and green numbers in parentheses indicate the mean errors for the Antarctic and Alaskan sites, respectively. The black solid and dashed lines represent the line of identity and the deviation of ±10 %, respectively. (Lower row) Probability distribution of the errors in ALT estimated with ASM for the depth pairs of 5/30 cm, 5/50 cm and 30/50 cm.

5 Discussion

5.1 Model performances

ASMs given by Eq. (8) and (27) reproduced MAPT and ALT with a reasonable accuracy under most idealized scenarios and field conditions, which corroborated their theoretical assumptions (see Sect. 2.1 and 2.2) and suggested that they can work reasonably well under a wide range of climates and ground physical conditions.

5.1.1 Mean annual permafrost table temperature

MAPT estimates by Eq. (8) had high accuracy regardless of the stratigraphy of the active layer and the depth pairs used for the calculations (Table 3, Fig. 3). Under idealized scenarios, the ASM deviations in the one-layer profiles were negligible, while in the two-layer profiles the temperatures were underestimated by less than ∼0.1 °C on average (Table 3). Under field conditions, the ASM deviations were close to zero on average, and the majority of them was below ±0.2 °C at the Antarctic and Alaskan sites (Fig. 3), which is within the accuracy of many temperature sensors and similar or better than in most previous studies that used other analytical or statistical models for MAPT estimates (e.g., Romanovsky and Osterkamp, 1995; Sazonova and Romanovsky, 2003; Ferreira et al., 2017; Way and Lewkowicz, 2018; Wang et al., 2020; Kaplan Pastíriková et al., 2023). This

https://doi.org/10.5194/egusphere-2024-2989
Preprint. Discussion started: 18 October 2024

is likely because the relationship between the thawing and freezing indices is linear within each subsurface layer, and its slope varies rather slightly with vertical changes in ground physical properties at the layer interfaces (Fig. 2). This was noticeable at the Alaskan sites where the presence of peat over mineral soil is common. So far, MAPT models have also typically assumed that thawed thermal conductivity is lower than frozen one, and that the thermal offset is therefore negativ (e.g., Gisnås et al., 2013; Obu et al., 2019, 2020), which would, however, yield invalid MAPT estimates under reverse conditions. Since Eq. (8) utilizes measured temperatures, it can easily handle even such anomalies, as demonstrated, for example, in McMurdo Sound where the thermal offset is often positive (Lacelle et al., 2016). Additionally, the thermal offset is usually in the order of tenths to first degrees Celsius and decreases exponentially with depth (Goodrich, 1982; Burn and Smith, 1988; Romanovsky and Osterkamp, 1995). Hence, it was relatively small below the bottom temperature sensors used for the calculations and MAPT estimates were subject to relatively small uncertainties. Somewhat larger deviations in MAPT estimates would, however, be expected in warmer conditions with thicker active layers and high vertical changes in ground physical properties.

5.1.2 Active-layer thickness

By contrast, ALT estimates by Eq. (27) had very different accuracy in the one-layer and two-layer profiles that also depended on the depth pairs used for the calculations (Table 4, Fig. 5). Under idealized scenarios, the ASM deviations in the one-layer profiles were below 1.5 % on average, while in the two-layer profiles the deviations were up to tens of percent, except for the depth pair of 30/50 cm, which excluded the thawing index from the top peat layer with different physical properties (Table 4). The minor deviations in the one-layer profiles and in the two-layer profiles for the depth pair of 30/50 cm were largely because the vertical profiles of the square-rooted thawing indices were not perfectly linear near the base of the active layer (Fig. 4), which was likely due to upward freezing from the permafrost table at the end of the thawing seasons (cf. Riseborough, 2003). Under field conditions, the ASM deviations were scattered around zero at the Antarctic sites and roughly attained less than 7 % on average, while ALT tended to be underestimated at the Alaskan sites by up to 14 % on average (Fig. 5). Overall, however, the accuracy of ASM given by Eq. (27) was similar or better than in most previous studies that used the other analytical or statistical models for ALT estimates (Anisimov et al., 1997; Nelson et al., 1997; Romanovsky and Osterkamp, 1997; Anisimov et al., 2002; Shiklomanov and Nelson, 2002; Sazonova and Romanovsky, 2003; Streletskiy et al., 2012; Yin et al., 2016; Zorigt et al., 2016; Hrbáček and Uxa, 2020; Kaplan Pastíriková et al., 2023). The higher accuracy of ASM at the Antarctic sites (Fig. 5) was likely due to the fact that the active layer there is relatively homogeneous in terms of its stratigraphy and physical properties, whereas at the Alaskan sites it typically consists of two distinct layers. This is also why the depth pair of 30/50 cm showed the lowest errors (Fig. 5), as it excluded the surface layer of peat, which is an effective thermal insulator that substantially alters the temperature gradient in the active layer.

5.2 Model advantages

Unlike other analytical or statistical models for estimating MAPT (e.g., Garagulya, 1990; Romanovsky and Osterkamp, 1995; Smith and Riseborough, 1996) and ALT (e.g., Neumann, c. 1860; Stefan, 1891; Kudryavtsev et al., 1977), ASMs given by Eq. (8) and (27) can be utilized in any substrates where conductive heat transfer prevails, such as soil, peat, or solid rock,

https://doi.org/10.5194/egusphere-2024-2989
Preprint. Discussion started: 18 October 2024

without the knowledge of their physical properties. Since ASMs build solely on thawing and freezing indices at two distinct depths in the active layer, the values of which reflect the rate of heat transfer across their intermediate layer, the solutions also intrinsically account for the temporal variability of ground physical properties. Likewise, they consider latent and sensible heat and any other factors that might affect the heat transfer in the active layer, some of which other models do not explicitly account for. This is highly convenient because data on ground physical properties, such as thermal conductivity, heat capacity, water content or bulk density, are not readily available at many sites. Ground physical properties for other models estimating MAPT (e.g., Gisnås et al., 2013; Obu et al., 2019, 2020; Garibaldi et al., 2021) and ALT (e.g., Hinkel and Nicholas, 1995; Nelson et al., 1997; Anisimov et al., 2002; Shiklomanov and Nelson, 2002) have been set empirically or have been based on published values, and therefore their values have frequently been of unknown validity. Ground physical properties also commonly show more or less variability on seasonal and annual time scales (e.g., Gao et al., 2020; Hrbáček et al., 2023a; Li et al., 2023; Kňažková and Hrbáček, 2024; Wenhao et al., 2024), which most other models cannot handle because they typically treat ground physical properties as constants.

Another advantage is that ASMs are not limited to temperatures at certain depths, but their inputs can be any depth combinations from within the active layer based on temperature data availability and site characteristics. For best MAPT and ALT estimates, it is therefore suggested to use thawing and freezing indices from depths as close as possible to the permafrost table, where available.

Besides field measurements, ASMs can also be forced by diverse climate reanalysis or climate model outputs, if these at least partially consider the physics of ground thawing and freezing. These products typically provide only ground surface and shallow active-layer temperatures with limited or no information on ground physical properties, which is frequently insufficient to determine MAPT and ALT either directly or using conventional solutions. However, this is not an issue for ASMs.

Lastly, ASMs can also be easily reformulated to be used for estimating the mean annual temperature at the base of seasonally frozen ground and frost depth (see Appendix A and B).

5.3 Model limitations

Since ASMs assume homogeneous (one-layer) profiles, they may understate reality in multi-layer profiles that exhibit large stepwise vertical changes in ground physical properties and/or higher ground-ice contents near the base of the active layer (Riseborough, 2003). If, for instance, temperature measurements are used only from the top layer, the physical properties of which differ from those of the layer below, ASMs may therefore be inaccurate (Fig. 2 and 4). Equally, the outputs may have unknown validity if only shallow temperature measurements in thick active layers are used because they would be based on the rate of heat transfer in a tiny portion of the active layer, which may differ in its deeper sections (Fig. 2 and 4). On the other hand, natural variability of ground physical properties with no sharp changes in their vertical distribution is unlikely to affect ASMs substantially. Other downside of ASMs is that they require temperature measurements at two depths in the active layer, which may not be available at many sites, and can also be problematic to collect if the active layer is thin. Special care must also be taken with the depths of the temperature sensors and the vertical distances between them, which must be constant over time, as well as with the accuracy of the sensors, because any deviations in these may negatively influence the ASMs

https://doi.org/10.5194/egusphere-2024-2989
Preprint. Discussion started: 18 October 2024

outputs. Nevertheless, these issues are largely common to any analytical, statistical and even numerical permafrost models, as they relate to the quality of the inputs rather than the shortcomings of ASMs themselves.

6 Conclusions

We devised two novel ASMs given by Eq. (8) and (27) for estimating MAPT and ALT, respectively, which are driven solely by pairwise combinations of thawing and freezing indices in the active layer; no ground physical properties are required. ASMs reproduced MAPT and ALT well under most idealized scenarios, which corroborated their theoretical assumptions. Under field conditions of Antarctica and Alaska, the mean ASMs deviations in MAPT and ALT were less than 0.03 °C and 5 %, respectively, which is very promising because it is similar or better than other analytical or statistical models. ASMs worked best in homogeneous active layers with small vertical changes in ground physical properties and when permafrost table was close below the temperature sensors considered for MAPT and ALT calculations.

Hence, ASMs for estimating MAPT and ALT can find applications under a wide range of climates and ground physical conditions wherever at least two temperature measurements in the active layer are available. Besides field measurements, they can also utilize diverse climate reanalyses or climate model ground temperature products. Lastly, they can be easily reformulated for estimating the mean annual temperature at the base of seasonally frozen ground and frost depth.

Appendix A: Derivation of ASM for mean annual temperature at the base of seasonally frozen ground

Similarly to Eq. (1), the mean annual temperature at the base of seasonally frozen ground (MASFT $> 0\,°C$) is calculated as follows (Romanovsky and Osterkamp, 1995)

$$\text{MASFT} = \frac{I_{ts} - \frac{k_f}{k_t} I_{fs}}{P}, \tag{A1}$$

which has the same attributes as Eq. (1). Hence, MASFT based on temperatures measured at two distinct depths in the seasonally freezing layer z_1 and z_2 ($z_1 < z_1 <$ FD) can be expressed as follows

$$\text{MASFT} = \frac{I_{tz_1} - \frac{k_f}{k_t} I_{fz_1}}{P}, \tag{A2}$$

$$\text{MASFT} = \frac{I_{tz_2} - \frac{k_f}{k_t} I_{fz_2}}{P}. \tag{A3}$$

This implies that Eq. (A2) and (A2) are equivalent:

$$\frac{I_{tz_1} - \frac{k_f}{k_t} I_{fz_1}}{P} = \frac{I_{tz_2} - \frac{k_f}{k_t} I_{fz_2}}{P}. \tag{A4}$$

Solving Eq. (A4) for the inverse of the thermal conductivity ratio yields

$$\frac{k_f}{k_t} = \frac{I_{tz_1} - I_{tz_2}}{I_{fz_1} - I_{fz_2}}. \tag{A5}$$

https://doi.org/10.5194/egusphere-2024-2989
Preprint. Discussion started: 18 October 2024

Equation (A5) can be then substituted for the thermal conductivity ratio in Eq. (A2) and (A3) as follows

$$\mathrm{MASFT} = \frac{I_{tz_1} - \frac{I_{tz_1} - I_{tz_2}}{I_{fz_1} - I_{fz_2}} I_{fz_1}}{P}, \tag{A6}$$

$$\mathrm{MASFT} = \frac{I_{tz_2} - \frac{I_{tz_1} - I_{tz_2}}{I_{fz_1} - I_{fz_2}} I_{fz_2}}{P}. \tag{A7}$$

Subsequently, Eq. (A6) and (A7) both simplify to the same formula for MASFT:

$$\mathrm{MASFT} = \frac{\frac{I_{fz_1} I_{tz_2} - I_{fz_2} I_{tz_1}}{I_{fz_1} - I_{fz_2}}}{P}, \tag{A8}$$

which only slightly differs from Eq. (A8) and has the same attributes.

Appendix B: Derivation of ASM for frost depth

Similarly to Eq. (13), frost depth (FD) can be calculated by the Stefan (1891) model as follows

$$\mathrm{FD} = \sqrt{\frac{2 k_f I_{fs}}{L \phi}}. \tag{B1}$$

Likewise, note that the freezing index must be multiplied by the scaling factor of 86 400 s d^{-1} in the Stefan model to yield correct outputs. FD estimated using freezing indices measured at two distinct depths z_1 and z_2 ($z_1 < z_1 <$FD) can be expressed as follows

$$\mathrm{FD} = z_1 + \sqrt{\frac{2 k_f I_{fz_1}}{L \phi}}, \tag{B2}$$

$$\mathrm{FD} = z_2 + \sqrt{\frac{2 k_f I_{fz_2}}{L \phi}}. \tag{B3}$$

This implies that Eq. (B2) and (B3) are equivalent:

$$z_1 + \sqrt{\frac{2 k_f I_{fz_1}}{L \phi}} = z_2 + \sqrt{\frac{2 k_f I_{fz_2}}{L \phi}}. \tag{B4}$$

The vertical distance between z_2 and z_1 can be expressed as

$$z_2 - z_1 = \sqrt{\frac{2 k_f I_{fz_1}}{L \phi}} - \sqrt{\frac{2 k_f I_{fz_2}}{L \phi}}, \tag{B5}$$

which simplifies to

$$z_2 - z_1 = \sqrt{\frac{2 k_f}{L \phi}} \left(\sqrt{I_{fz_1}} - \sqrt{I_{fz_2}} \right). \tag{B6}$$

https://doi.org/10.5194/egusphere-2024-2989
Preprint. Discussion started: 18 October 2024

Subsequently rearranging Eq. (B6) gives

$$\frac{z_2 - z_1}{\sqrt{I_{fz_1}} - \sqrt{I_{fz_2}}} = \sqrt{\frac{2k_f}{L\phi}}, \tag{B7}$$

where the right-hand side corresponds to the edaphic term, which combines the ground physical properties in the Stefan model into a single variable. The edaphic term can be implemented in Eq. (B2) and (B2) as follows

$$\mathrm{FD} = z_1 + E\sqrt{I_{fz_1}}, \tag{B8}$$

$$\mathrm{FD} = z_2 + E\sqrt{I_{fz_2}}. \tag{B9}$$

Substituting the left-hand side of Eq. (B7) for the edaphic term in Eq. (B8) and (B9) yields

$$\mathrm{FD} = z_1 + \frac{z_2 - z_1}{\sqrt{I_{fz_1}} - \sqrt{I_{fz_2}}}\sqrt{I_{fz_1}}, \tag{B10}$$

$$\mathrm{FD} = z_2 + \frac{z_2 - z_1}{\sqrt{I_{fz_1}} - \sqrt{I_{fz_2}}}\sqrt{I_{fz_2}}. \tag{B11}$$

Simplifying Eq. (B10) and (B11) then produces the same formula for FD:

$$\mathrm{FD} = \frac{z_2\sqrt{I_{fz_1}} - z_1\sqrt{I_{fz_2}}}{\sqrt{I_{fz_1}} - \sqrt{I_{fz_2}}}, \tag{B12}$$

which is the same and has the same attributes as Eq. (27), only the freezing indices are used instead of the thawing ones.

Data availability. The validation datasets from James Ross Island are available upon request from Filip Hrbáček (hrbacekfilip@gmail.com), whereas those from McMurdo Sound and North Slope of Alaska can be retrieved from https://www.nrcs.usda.gov/resources/data-and-reports/soil-climate-research-stations.

Author contributions. TU: conceptualization, methodology, software, validation, formal analysis, investigation, writing – original draft, visualization. FH: conceptualization, resources, writing – review & editing, supervision, funding acquisition. MK: formal analysis, resources, writing – review & editing.

Competing interests. The contact author has declared that none of the authors has any competing interests.

Acknowledgements. We acknowledge USDA for access to the soil climate data from the McMurdo Sound and North Slope of Alaska.

Financial support. The research was funded by the Czech Science Foundation (project number GM22-28659M).

https://doi.org/10.5194/egusphere-2024-2989
Preprint. Discussion started: 18 October 2024

References

Aalto, J., Karjalainen, O., Hjort, J., and Luoto, M.: Statistical forecasting of current and future Circum-Arctic ground temperatures and active layer thickness, Geophys. Res. Lett., 45, 4889–4898, 2018.

Anisimov, O. A., Shiklomanov, N. I., and Nelson, F. E.: Global warming and active-layer thickness: results from transient general circulation models, Glob. Planet. Change, 15, 61–77, https://doi.org/10.1016/S0921-8181(97)00009-X, 1997.

Anisimov, O. A., Shiklomanov, N. I., and Nelson, F. E.: Variability of seasonal thaw depth in permafrost regions: a stochastic modeling approach, Ecol. Model., 153, 217–227, https://doi.org/10.1016/S0304-3800(02)00016-9, 2002.

Biskaborn, B. K., Lanckman, J.-P., Lantuit, H., Elger, K., Streletskiy, D. A., Cable, W. L., and Romanovsky, V. E.: The new database of the Global Terrestrial Network for Permafrost (GTN-P), Earth Syst. Sci. Data, 7, 245–259, https://doi.org/10.5194/essd-7-245-2015, 2015.

Biskaborn, B. K., Smith, S. L., Noetzli, J., Matthes, H., Vieira, G., Streletskiy, D. A., Schoeneich, P., Romanovsky, V. E., Lewkowicz, A. G., Abramov, A., Allard, M., Boike, J., Cable, W. L., Christiansen, H. H., Delaloye, R., Diekmann, B., Drozdov, D., Etzelmüller, B., Grosse, G., Guglielmin, M., Ingeman-Nielsen, T., Isaksen, K., Ishikawa, M., Johansson, M., Johansson, H., Joo, A., Kaverin, D., Kholodov, A., Konstantinov, P., Kröger, T., Lambiel, C., Lanckman, J.-P., Luo, D., Malkova, G., Meiklejohn, I., Moskalenko, N., Oliva, M., Phillips, M., Ramos, M., Sannel, A. B. K., Sergeev, D., Seybold, C., Skryabin, P., Vasiliev, A., Wu, Q., Yoshikawa, K., Zheleznyak, M., and Lantuit, H.: Permafrost is warming at a global scale, Nat. Commun., 10, 264, https://doi.org/10.1038/s41467-018-08240-4, 2019.

Bonnaventure, P. P. and Lamoureux, S. F.: The active layer: A conceptual review of monitoring, modelling techniques and changes in a warming climate, Prog. Phys. Geog., 37, 352–376, https://doi.org/10.1177/0309133313478314, 2013.

Brown, J., Hinkel, K. M., and Nelson, F. E.: The circumpolar active layer monitoring (calm) program: Research designs and initial results, Polar Geogr., 24, 166–258, https://doi.org/10.1080/10889370009377698, 2000.

Burn, C. R.: The Active Layer: Two Contrasting Definitions, Permafrost Periglac., 9, 411–416, https://doi.org/10.1002/(SICI)1099-1530(199810/12)9:4<411::AID-PPP292>3.0.CO;2-6, 1998.

Burn, C. R. and Smith, C. A. S.: Observations of the "Thermal Offset" in Near-Surface Mean Annual Ground Temperatures at Several Sites near Mayo, Yukon Territory, Canada, Arctic, 41, 99–104, https://www.jstor.org/stable/40510685, 1988.

Carslaw, H. S. and Jaeger, J. C.: Conduction of Heat in Solids, Second Edition, Oxford University Press, Oxford, United Kingdom, 520 pp., 1959.

de Pablo, M. A., Ramos, M., Molina, A., and Prieto, M.: Thaw depth spatial and temporal variability at the Limnopolar Lake CALM-S site, Byers Peninsula, Livingston Island, Antarctica, Sci. Total Environ., 615, 814–827, https://doi.org/10.1016/j.scitotenv.2017.09.284, 2018.

Farzamian, M., Vieira, G., Monteiro Santos, F. A., Yaghoobi Tabar, B., Hauck, C., Paz, M. C., Bernardo, I., Ramos, M., and de Pablo, M. A.: Detailed detection of active layer freeze–thaw dynamics using quasi-continuous electrical resistivity tomography (Deception Island, Antarctica), The Cryosphere, 14, 1105–1120, https://doi.org/10.5194/tc-14-1105-2020, 2020.

Ferreira, A., Vieira, G., Ramos, M., and Nieuwendam, A.: Ground temperature and permafrost distribution in Hurd Peninsula (Livingston Island, Maritime Antarctic): An assessment using freezing indexes and TTOP modelling, Catena, 149, 560–571, http://dx.doi.org/10.1016/j.catena.2016.08.027, 2017.

Gao, Z., Lin, Z., Niu, F., and Luo, J.: Soil water dynamics in the active layers under different land-cover types in the permafrost regions of the Qinghai–Tibet Plateau, China. Geoderma, 364, 114176, https://doi.org/10.1016/j.geoderma.2020.114176, 2020.

Garagulya, L. S.: Application of Mathematical Methods and Computers in Investigations of Geocryological Processes, Moscow University Press, Moscow, Russia, 124 pp., 1990.

https://doi.org/10.5194/egusphere-2024-2989
Preprint. Discussion started: 18 October 2024

Garibaldi, M. C., Bonnaventure, P. P., and Lamoureux, S. F.: Utilizing the TTOP model to understand spatial permafrost temperature variability in a High Arctic landscape, Cape Bounty, Nunavut, Canada, Permafrost Periglac., 32, 19–34, https://doi.org/10.1002/ppp.2086, 2021.

Gisnås, K., Etzelmüller, B., Farbrot, H., Schuler, T. V., and Westermann, S.: CryoGRID 1.0: Permafrost Distribution in Norway estimated by a Spatial Numerical Model, Permafrost Periglac., 24, 2–19, https://doi.org/10.1002/ppp.1765, 2013.

Goodrich, L. E.: The influence of snow cover on the ground thermal regime, Can. Geotech. J., 19, 421–432, https://doi.org/10.1139/t82-047, 1982.

Grosse, G., Goetz, S., McGuire, A. D., Romanovsky, V. E., and Schuur, E. A. G.: Changing permafrost in a warming world and feedbacks to the Earth system, Environ. Res. Lett., 11, 040201, https://doi.org/10.1088/1748-9326/11/4/040201, 2016.

Hauck, C.: Frozen ground monitoring using DC resistivity tomography, Geophys. Res. Lett., 29, 2016, https://doi.org/10.1029/2002GL014995, 2002.

Hayashi, M., Goeller, N., Quinton, W. L., and Wright, N.: A simple heat-conduction method for simulating the frost-table depth in hydrological models, Hydrol. Process., 21, 2610–2622, https://doi.org/10.1002/hyp.6792, 2007.

Hinkel, K. M., Nicholas, J. R. J.: Active Layer Thaw Rate at a Boreal Forest Site in Central Alaska, U.S.A., Arct. Alp. Res., 27, 72–80, https://doi.org/10.2307/1552069, 1995.

Hjort, J., Streletskiy, D., Doré, G., Wu, Q., Bjella, K., and Luoto, M.: Impacts of permafrost degradation on infrastructure, Nat. Rev. Earth Environ., 3, 24–38, https://doi.org/10.1038/s43017-021-00247-8, 2022.

Hrbáček, F. and Uxa, T.: The evolution of a near-surface ground thermal regime and modeled active-layer thickness on James Ross Island, Eastern Antarctic Peninsula, in 2006–2016, Permafrost Periglac., 31, 141–155, https://doi.org/10.1002/ppp.2018, 2020.

Hrbáček, F., Kňažková, M., Farzamian, M., and Baptista, J.: Variability of soil moisture on three sites in the Northern Antarctic Peninsula in 2022/23, Czech Polar Rep., 13, 10–23, https://doi.org/10.5817/CPR2023-1-2, 2023a.

Hrbáček, F., Oliva, M., Hansen, C., Balks, M., O'Neill, T. A., de Pablo, M. A., Ponti, S., Ramos, M., Vieira, G., Abramov, A., Kaplan Pastíriková, L., Guglielmin, M., Goyanes, G., Rocha Francelino, M., Schaefer, C., and Lacelle, D.: Active layer and permafrost thermal regimes in the ice-free areas of Antarctica, Earth-Sci. Rev., 242, 104458, https://doi.org/10.1016/j.earscirev.2023.104458, 2023b.

Kaplan Pastíriková, L., Hrbáček, F., Uxa, T., and Láska, K.: Permafrost table temperature and active layer thickness variability on James Ross Island, Antarctic Peninsula, in 2004–2021, Sci. Total Environ., 869, 161690, https://doi.org/10.1016/j.scitotenv.2023.161690, 2023.

Kňažková, M. and Hrbáček, F.: Interannual variability of soil thermal conductivity and moisture on the Abernethy Flats (James Ross Island) during thawing seasons 2015–2023, Catena, 234, 107640, https://doi.org/10.1016/j.catena.2023.107640, 2024.

Kudryavtsev, V. A., Garagulia, L., Kondratyeva, K. A., and Melamed, V. G.: Fundamentals of Frost Forecasting in Geological Engineering Investigations, Draft Translation 606, U.S. Army Cold Regions Research And Engineering Lab, Hanover, NH, 489 pp., 1977.

Kurylyk, B. L.: Discussion of 'A Simple Thaw-Freeze Algorithm for a Multi-Layered Soil using the Stefan Equation' by Xie and Gough (2013), Permafrost Periglac., 26, 200–206, https://doi.org/10.1002/ppp.1834, 2015.

Lacelle, D., Lapalme, C., Davila, A. F., Pollard, W., Marinova, M., Heldmann, J., and McKay, C. P.: Solar radiation and air and ground temperature relations in the cold and hyper-arid Quartermain Mountains, McMurdo Dry Valleys of Antarctica, Permafrost Periglac., 27, 163–176, https://doi.org/10.1002/ppp.1859, 2016.

Lawrence, D. M., Koven, C. D., Swenson, S. C., Riley, W. J., and Slater, A. G.: Permafrost thaw and resulting soil moisture changes regulate projected high-latitude CO_2 and CH_4 emissions, Environ. Res. Lett., 10, 094011, https://doi.org/10.1088/1748-9326/10/9/094011, 2015.

https://doi.org/10.5194/egusphere-2024-2989
Preprint. Discussion started: 18 October 2024

Li, G., Zhang, M., Pei, W., Melnikov, A., Khristoforov, I., Li, R., and Yu, F.: Changes in permafrost extent and active layer thickness in the Northern Hemisphere from 1969 to 2018, Sci. Total Environ., 804, 150182, https://doi.org/10.1016/j.scitotenv.2021.150182, 2022.

Li, W., Weng, B., Yan, D., Lai, Y., Li, M., and Wang, H.: Underestimated permafrost degradation: Improving the TTOP model based on soil thermal conductivity, Sci. Total Environ., 854, 158564, https://doi.org/10.1016/j.scitotenv.2022.158564, 2023.

Lunardini, V. J.: Theory of N-factors and correlation of data, in: Proceedings of the 3rd International Conference on Permafrost, Edmonton, Canada, 10–13 July 1978, 40–46, 1978.

Lunardini, V. J.: Heat Transfer in Cold Climates, Van Nostrand Reinhold Co., New York, NY, 731 pp., 1981.

Nelson, F. E. and Outcalt, S. I.: A Computational Method for Prediction and Regionalization of Permafrost, Arctic Alpine Res., 19, 279–288, https://doi.org/10.2307/1551363, 1987.

Nelson, F. E., Shiklomanov, N. I., Mueller, G., Hinkel, K. M., Walker, D. A., and Bockheim, J. G.: Estimating Active-Layer Thickness over a Large Region: Kuparuk River Basin, Alaska, U.S.A., Arct. Alp. Res., 29, 367–378, https://doi.org/10.2307/1551985, 1997.

Neumann, F.: Lectures given in the 1860's, cf. Riemann-Weber, Die Partiellen Differentialgleichungen der Mathematischen, Physik, 2, 117–121.

Nicolsky, D. J., Romanovsky, V. E., and Panteleev, G. G.: Estimation of soil thermal properties using in-situ temperature measurements in the active layer and permafrost, Cold Reg. Sci. Technol., 55, 120–129, https://doi.org/10.1016/j.coldregions.2008.03.003, 2009.

Noetzli, J., Arenson, L. U., Bast, A., Beutel, J., Delaloye, R., Farinotti, D., Gruber, S., Gubler, H., Haeberli, W., Hasler, A., Hauck, C., Hiller, M., Hoelzle, M., Lambiel, C., Pellet, C., Springman, S. M., Vonder Muehll, D., and Phillips, M.: Best Practice for Measuring Permafrost Temperature in Boreholes Based on the Experience in the Swiss Alps, Front. Earth Sci., 9, 607875, https://doi.org/10.3389/feart.2021.607875, 2021.

Noetzli, J., Christiansen, H. H., Guglielmin, M., Hrbáček, F., Hu, G., Isaksen, K., Magnin, F., Pogliotti, P., Smith, S. L., Zhao, L., and Streletskiy, D. A.: Permafrost temperature and active-layer thickness, in: State of the Climate in 2023, Bull. Amer. Meteor. Soc., 105, S43–S44. https://doi.org/10.1175/2024BAMSStateoftheClimate.1, 2024.

Obu, J.: How Much of the Earth's Surface is Underlain by Permafrost?, J. Geophys. Res.–Earth, 126, e2021JF006123, https://doi.org/10.1029/2021JF006123, 2021.

Obu, J., Westermann, S., Bartsch, A., Berdnikov, N., Christiansen, H. H., Dashtseren, A., Delaloye, R., Elberling, B., Etzelmüller, B., Kholodov, A., Khomutov, A., Kääb, A., Leibman, M. O., Lewkowicz, A. G., Panda, S. K., Romanovsky, V., Way, R. G., Westergaard-Nielsen, A., Wu, T., Yamkhin, J., and Zou, D.: Northern Hemisphere permafrost map based on TTOP modelling for 2000–2016 at 1 km^2 scale, Earth Sci. Rev., 193, 299–316, https://doi.org/10.1016/j.earscirev.2019.04.023, 2019.

Obu, J., Westermann, S., Vieira, G., Abramov, A., Balks, M. R., Bartsch, A., Hrbáček, F., Kääb, A., and Ramos, M.: Pan-Antarctic map of near-surface permafrost temperatures at 1 km^2 scale, The Cryosphere, 14, 497–519, https://doi.org/10.5194/tc-14-497-2020, 2020.

Peng, X., Zhang, T., Frauenfeld, O. W., Mu, C., Wang, K., Wu, X., Guo, D., Luo, J., Hjort, J., Aalto, J., Karjalainen, O., and Luoto, M.: Active Layer Thickness and Permafrost Area Projections for the 21st Century, Earth's Future, 11, e2023EF003573, https://doi.org/10.1029/2023EF003573, 2023.

Riseborough, D.: Thawing and freezing indices in the active layer, in: Proceedings of the 8th International Conference on Permafrost, Zurich, Switzerland, 21–25 July 2003, 953-–958, 2003.

Riseborough, D., Shiklomanov, N., Etzelmüller, B., Gruber, S., and Marchenko, S.: Recent advances in permafrost modelling, Permafrost Periglac., 19, 137–156, https://doi.org/10.1002/ppp.615, 2008.

https://doi.org/10.5194/egusphere-2024-2989
Preprint. Discussion started: 18 October 2024

Romanovsky, V. E. and Osterkamp, T. E.: Interannual Variations of the Thermal Regime of the Active Layer and Near-Surface Permafrost in Northern Alaska, Permafrost Periglac., 6, 313–335, https://doi.org/10.1002/ppp.3430060404, 1995.

Romanovsky, V. E. and Osterkamp, T. E.: Thawing of the Active Layer on the Coastal Plain of the Alaskan Arctic, Permafrost Periglac., 8, 1–22, https://doi.org/10.1002/(SICI)1099-1530(199701)8:1<1::AID-PPP243>3.0.CO;2-U, 1997.

Sazonova, T. S. and Romanovsky, V. E.: A model for regional-scale estimation of temporal and spatial variability of active layer thickness and mean annual ground temperaturesPermafrost Periglac., 14, 125–139, https://doi.org/10.1002/ppp.449, 2003.

Schuur, E. A., Abbott, B. W., Commane, R., Ernakovich, J., Euskirchen, E., Hugelius, G., Grosse, G., Jones, M., Koven, C., Leshyk, V., Lawrence, D., Loranty, M. M., Mauritz, M., Olefeldt, D., Natali, S., Rodenhizer, H., Salmon, V., Schädel, C., Strauss, J., Treat, C., and Turetsky, M.: Permafrost and Climate Change: Carbon Cycle Feedbacks From the Warming Arctic, Annu. Rev. Env. Resour., 47, 343–371, https://doi.org/10.1146/annurev-environ-012220-011847, 2022.

Shiklomanov, N. I. and Nelson, F. E.: Active-Layer Mapping at Regional Scales: A 13-Year Spatial Time Series for the Kuparuk Region, North-Central Alaska, Permafrost Periglac., 13, 219–230, https://doi.org/10.1002/ppp.425, 2002.

Shiklomanov, N. I., Streletskiy, D. A., Nelson, F. E., Hollister, R. D., Romanovsky, V. E., Tweedie, C. E., Bockheim, J. G., and Brown, J.: Decadal variations of active-layer thickness in moisture-controlled landscapes, Barrow, Alaska, J. Geophys. Res.-Biogeo., 115, G00I04, https://doi.org/10.1029/2009JG001248, 2010.

Smith, M. W. and Riseborough, D. W.: Permafrost monitoring and detection of climate change, Permafrost Periglac., 7, 301–309, https://doi.org/10.1002/(SICI)1099-1530(199610)7:4<301::AID-PPP231>3.0.CO;2-R, 1996.

Smith, S. L., O'Neill, H. B., Isaksen, K., Noetzli, J., and Romanovsky, V. E.: The changing thermal state of permafrost, Nat. Rev. Earth Environ., 3, 10–23, https://doi.org/10.1038/s43017-021-00240-1, 2022.

Stefan, J.: Über die Theorie der Eisbildung, insbesondere über die Eisbildung im Polarmeere, Ann. Phys., 278, 269–286, https://doi.org/10.1002/andp.18912780206, 1891.

Streletskiy, D. A., Shiklomanov, N. I., and Nelson, F. E.: Spatial variability of permafrost active-layer thickness under contemporary and projected climate in northern Alaska, Polar Geogr., 35, 95–116, https://doi.org/10.1080/1088937X.2012.680204, 2012.

Sun, Z., Zhao, L., Hu, G., Qiao, Y., Du, E., Zou, D., and Xie, C.: Modeling permafrost changes on the Qinghai-Tibetan plateau from 1966 to 2100: A case study from two boreholes along the Qinghai-Tibet engineering corridor, Permafrost Periglac., 31, 156–171, https://doi.org/10.1002/ppp.2022, 2020.

Walvoord, M. A., Kurylyk, B.L.: Hydrologic Impacts of Thawing Permafrost—A Review, Vadose Zone J., 15, vzj2016-01, https://doi.org/10.2136/vzj2016.01.0010, 2016.

Wang, C., Wang, Z., Kong, Y., Zhang, F., Yang, K., and Zhang, T.: Most of the Northern Hemisphere Permafrost Remains under Climate Change, Sci. Rep., 9, 3295, https://doi.org/10.1038/s41598-019-39942-4, 2019.

Wang, K., Jafarov, E., and Overeem, I.: Sensitivity evaluation of the Kudryavtsev permafrost model, Sci. Total Environ., 720, 137538, https://doi.org/10.1016/j.scitotenv.2020.137538, 2020.

Way, R. G. and Lewkowicz, A. G.: Environmental controls on ground temperature and permafrost in Labrador, northeast Canada, Permafrost Periglac., 29, 73–85, https://doi.org/10.1002/ppp.1972, 2018.

Wenhao, L., Ren, L., Tonghua, W., Xiaoqian, S., Xiaodong, W., Guojie, H., Lin, Z., Jimin, Y., Dong, W., Yao, X., Jianzong, S., Junjie, M., Shenning, W., and Yongping, Q.: Spatio-temporal variation in soil thermal conductivity during the freeze-thaw period in the permafrost of the Qinghai–Tibet Plateau in 1980–2020, Sci. Total Environ., 913, 169654, https://doi.org/10.1016/j.scitotenv.2023.169654, 2024.

https://doi.org/10.5194/egusphere-2024-2989
Preprint. Discussion started: 18 October 2024

Yin, G., Niu, F., Lin, Z., Luo, J., and Liu, M.: Performance comparison of permafrost models in Wudaoliang Basin, Qinghai-Tibet plateau, China, J. Mt. Sci., 13, 1162–1173, https://doi.org/10.1007/s11629-015-3745-x, 2016.

Zhao, S. P., Nan, Z. T., Huang, Y. B., and Zhao, L.: The Application and Evaluation of Simple Permafrost Distribution Models on the Qinghai–Tibet Plateau, Permafrost Periglac., 28, 391–404, https://doi.org/10.1002/ppp.1939, 2017.

Zorigt, M., Kwadijk, J., Van Beek, E., and Kenner, S.: Estimating thawing depths and mean annual ground temperatures in the Khuvsgul region of Mongolia, Environ. Earth Sci., 75, 897, https://doi.org/10.1007/s12665-016-5687-1, 2016.